Aqueous Solution Derived Amorphous Indium Doped Gallium Oxide Thin-Film Transistors

FUCHAO HE, YU QIN, YIFEI WANG, ZHENHUA LIN, JIE SU , JINCHENG ZHANG ,
JINGJING CHANG (Member, IEEE), AND YUE HAO (Senior Member, IEEE)

State Key Discipline Laboratory of Wide Band Gap Semiconductor Technology, Shaanxi Joint Key Laboratory of Graphene,
School of Microelectronics, Xidian University, Xi'an 710071, China

CORRESPONDING AUTHOR: J. CHANG (e-mail: jjingchang@xidian.edu.cn)

ABSTRACT In this study, we report high-performance amorphous Ga_2O_3 metal-oxide (AMO) thin film transistor (TFT) using an low-temperature solution-process coupling with In alloy engineering. In doping can lower the activation temperature of gallium oxide and increase the oxygen vacancy concentration to further activate the device. The optical bandgap of IGO film can be changed from 5.3 to 4.25 eV with the In doping concentration (C_{In}) increasing from 0 % to 50 %. All TFTs with IGO channels exhibit n-type transistor characteristics and the evolution of their key electrical parameters with the In-dopant is well elucidated by the structural and morphological characterization. With the increase of C_{In}, the performance of the device becomes better. Finally, a saturation field-effect mobility of 3.63 $cm^2V^{-1}s^{-1}$, a current on/off ratio of 10^6, and a threshold voltage of 2.5 V are achieved by the $In_{0.5}Ga_{0.5}O$ ($C_{In} = 50\%$) based device. The $In_{0.5}Ga_{0.5}O$ TFT also demonstrates good bias stress stability. Under the action of 20 V and -20 V gate bias for 3000 s, the ΔV_{TH} is $+2.27$ V and -1.95 V, respectively.

INDEX TERMS Thin film transistor (TFT), solution process, gallium oxide (Ga_2O_3), in doping.

I. INTRODUCTION

The requirement to grow oxide semiconductor films by low cost (easy-to-operate, large-area fabrication, non-vacuum) techniques has made solution process attractive in the past few years [1]–[6]. In the process of solution preparation, metal oxide semiconductor is more suitable for preparing transparent thin film transistor (TFT) circuits [7]–[8]. For all metal oxide materials, the empty metal cation s-states constitute the conduction band minimum. When the spatial overlap of metal s-states is bigger than the interaction distance of metal ions, the electron mobility of amorphous phase can be equivalent to or slightly lower than that of the corresponding single crystal. The main quantum number (n) mainly determines the spatial expansion of metal s-states, so the transition metal elements with $(n-1)d^{10}ns^0$ ($n \geq 5$) peripheral electronic arrangement, are ideal oxide semiconductor candidates [9], like In element

which satisfies this requirement. Further research has found that mixing metal cations with different sizes can effectively enhance thin film properties in multiple compounds, such as binary, ternary, or even quaternary components. So far, many researchers have studied that the AOS thin films fabricated by solution process could be employed to obtain high quality TFTs [3], [10]–[17]. For instance, electron mobilities larger than 2 cm^2 V^{-1} s^{-1} are obtained by the amorphous ZnO, IZO and Ga_2O_3 transistors [18]–[19]. However, the acquisition of outstanding performance depends on the high temperature, since these oxide films are usually annealed at a temperature larger than 450 °C.

Among these AOSs, Ga_2O_3 is a large band gap semiconductor with extremely high electric field strength which is higher than GaN and SiC [20]–[24], and hence, it exhibits great potential for various optoelectronic applications. Recently, compared to single crystal and bulk materials, the

Ga_2O_3 thin film has been increasingly of greater interest to researchers because of its low cost, easy growth, excellent repeatability, and flexibility. Various approaches have been employed to prepare β-Ga_2O_3 thin films, such as radio-frequency magnetron sputtering [25]–[26], molecular beam epitaxy, etc. However, solution processed β-Ga_2O_3 has less been reported due to the very high transition temperatures above 700 °C. Previously, Thomas et al. reported the ultrasonic spray pyrolysis method to grow β-Ga_2O_3 thin films, and achieved good performance TFTs by using Ca as the electrode [27].

Chemical doping is an effective approach to lower down the transition temperature. For example, Tobin et al. used Ga doping to lower down the ZnO transition temperature. Moreover, various doping methods have been used to control the film electrical properties [28]–[29]. In doping could introduce a large number of oxygen vacancies (V_O) and increase the carrier concentration of the thin film due to the weaker In-O bonding compared to Zn-O and Al-O bondings. Meanwhile, it has little effect on the lattice structure of Ga_2O_3. Hence, In is an appropriate doping source in the insulating Ga_2O_3 thin film to improve device performance. In this study, we propose aqueous solution-grown In doped Ga_2O_3 ($C_{In} \leq 50$ mol%) and elaborate the role of In doping in enabling low-cost, low-temperature, low-pollution and high-quality AOS thin films preparation. The electrical characteristics of TFTs based on Ga_2O_3 thin films with different In doping concentrations are compared in detail to clarify the influence of chemical composition and annealing temperature on the performance parameters of AOS-TFTs.

II. EXPERIMENT

The gallium nitrate $[Ga(NO_3)_3 \cdot xH_2O]$ powder and indium nitrate $[In(NO_3)_3 \cdot xH_2O]$ powder were dissolved in deionized (DI) water (10 mL) to obtain the corresponding precursor solutions. The molar ratios of In/(In+Ga) are 0 %, 5 %, 10 %, 25 % and 50 % respectively. To obtain the IGO films the precursor solution was spin coated at 3000 rpm for 30 s. These P^{++}-Si/SiO2/IGO samples were then annealed at 450 °C for 1h in ambient air. Finally, a 100 nm thick patterned Al (as source/drain electrodes) was thermally evaporated on the IGO films (W/L = 1000/100 μm). An Agilent 1500 semiconductor parameter analyzer was employed to obtain the thin film transistor characteristics in the dark at room temperature.

The surface roughness of the IGO films has been tested by Atomic force microscopy (AFM). The X-ray diffraction (XRD) was used to study the structural characteristics of the IGO films. Photoluminescence (PL) spectroscopy was measured with 325 nm He-Cd laser as excitation source. In order to explore the bandgap of IGO, a UV–visible spectrophotometer (UV-Vis) measurement was carried out. X-ray photoelectron spectroscopy (XPS) was also carried out to study the film composition.

The models of IGO were investigated by the VASP code using the Perdew–Burke–Ernzerhof (PBE) of Generalized
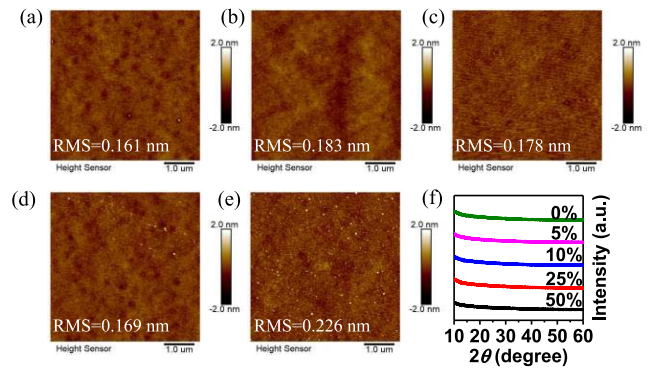

FIGURE 1. AFM images of IGO films with C_{In} of (a) 0 %, (b) 5 %, (c) 10 %, (d) 25 %, and (e) 50 %. (f) XRD patterns of the IGO thin films with different In concentrations.

gradient approximation (GGA) [30]–[32]. The $1 \times 3 \times 2$ super-cell models of β-Ga_2O_3 were employed to construct IGO with different concentration oxygen-vacancies. A plane-wave basis with energy cutoff of 400 eV and an energy convergence criterion of 10^{-5} eV were used to perform the geometry optimization. Meanwhile the d states of Ga were treated as the valence states. Just the gamma point was set for the geometry optimization calculations due to the large size of supercell.

The alloying formation enthalpies (ΔH) and vacancy formation energies (E_f) were calculated by the following formula [33]–[34]:

$$\Delta H\left[(In_xGa_{1-x})_2O_3\right] = E\left[(In_xGa_{1-x})_2O_3\right] \\ - xE[In_2O_3] - (1-x)E[Ga_2O_3] \quad (1)$$

$$E_f = E_w - E_{w/o} - n_o\mu_o \quad (2)$$

where $E[(In_xGa_{1-x})_2O_3]$, $E[In_2O_3]$, and $E[Ga_2O_3]$ were the total energies of $(In_xGa_{1-x})_2O_3$, In_2O_3, and Ga_2O_3 in the same supercell. The E_w and $E_{w/o}$ were respective the total energies of the IGO models with and without oxygen-vacancies. n_O and μ_O were respective the number and chemical potential of oxygen atom.

III. RESULTS AND DICUSSIONS

All films with a thickness of 5-10 nm are spin-coated from 0.1 M precursor solutions and then annealed at a selective temperature to ensure high-quality films. Figure 1 (a)-(e) exhibit the AFM images of IGO films deposited on the sapphire substrates. The root mean square (RMS) roughnesses of C_{In}-0%, C_{In}-5%, C_{In}-10%, C_{In}-25% and C_{In}-50% thin films are 0.161 nm, 0.183 nm, 0.178 nm, 0.169 nm and 0.226 nm, respectively. All films show sub-nanometer surface morphology. The extremely smooth IGO films can lead to a good quality of the interface area between the drain/source electrodes and the semiconductor layer, and then reduces the scattering effect. To further reveal the structure characters of these fabricated IGO films, the XRD curves are illustrated in Figure 1(f). None peaks are observed in
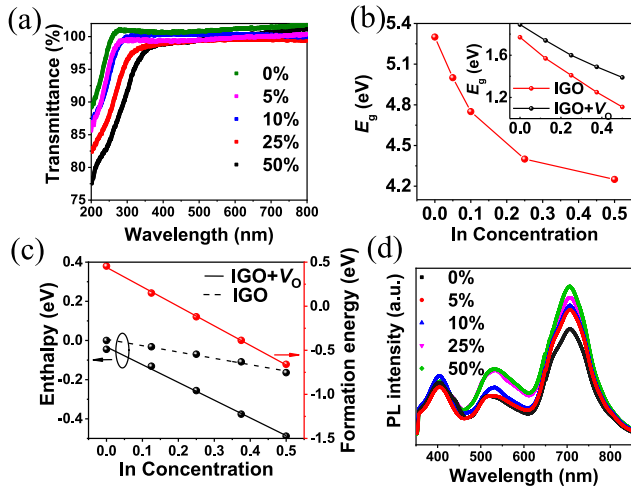
FIGURE 2. (a) The transmittance spectra for different C_{In} thin films on sapphire substrates. (b) The extracted direct bandgap (E_g) is plotted as a function of C_{In}. The line is drawn to show the variation trend. The inset panel gives the bandgap of IGO and IGO+V_O calculated by the DFT. (c) The formation enthalpies of IGO and IGO+V_O and O-vacancy formation energy in IGO. (d) Photoluminescence intensity profiles of the IGO thin films with different C_{In}.

FIGURE 3. O 1s XPS spectra for IGO films with C_{In} of (a) 0 %, (b) 5 %, (c) 10 %, (d) 25 % and (e) 50 % annealed at 450 °C. (f) Relative concentrations of M-O and Vo+ M-OH in the films with different In concentrations, as determined by XPS.

the Figure 1(f), regardless of the concentration of In component, suggesting that all fabricated films are amorphous. That is because the deposition and annealing temperatures are far lower than the crystallization temperature of β-Ga₂O₃ (> 700°C).

Figure 2(a) displays the transmittance spectra of the IGO films. It is seen that, all the films possess high transmittance over 97 % in the visible region and a sharp absorption edges in the deep ultraviolet region. The transmittance is reduced and the absorption edges blue-shifts with the increasing In concentration because the lower bandgap of In₂O₃ can reduce the bandgap of IGO alloys. The detailed bandgaps of IGO alloys are extrapolated through the ($\alpha h\nu$) plots using Tauc model [2], and listed in Figure 2(b). The bandgap reduces from 5.30 eV (C_{In}-0% Ga₂O₃) to 4.25 eV (C_{In}-50 %), demonstrating an effective variation of the bandgap of Ga₂O₃ by In-alloying. Note that, the bandgap of Ga₂O₃ film is larger than the band gap (4.6-4.9 eV) of β-Ga₂O₃ single crystal due to Burstein–Moss effect [35]. Meanwhile, the oxygen-vacancy may exist in the fabricated films, which can shift up the conduction band and then enlarges the bandgap, as displayed in Figure S1, in the supplementary material. The inset of Figure 2(b) lists the calculated band gap of IGO and IGO with an oxygen-vacancy (IGO+V_O). Obviously, the latter is higher than the former. To verify the existence of oxygen-vacancy, the formation enthalpies of IGO and IGO+V_O are calculated and displayed in Figure 2(c). The formation enthalpies of IGO+V_O are lower than those of IGO, suggesting the larger stability for the IGO+V_O than the IGO. Meanwhile, the formation energy of V_O in IGO is relative low, suggesting the spontaneous formation of V_O. Moreover, the alloying formation enthalpy and oxygen-vacancy formation energy decrease
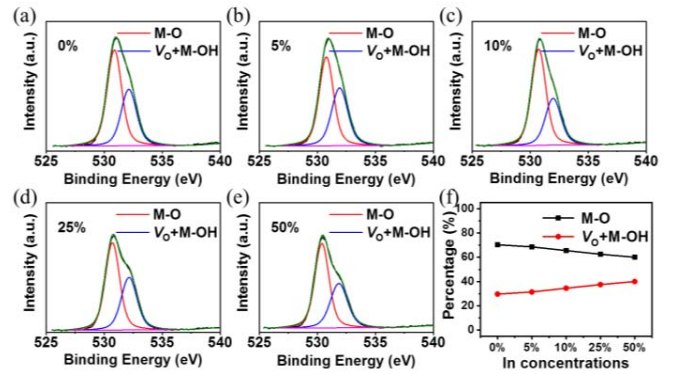
with the increasing In concentration. It means the enlarging oxygen-vacancy concentration when more and more In component is introduced into the Ga₂O₃ film. Figure 2(d) gives the photoluminescence (PL) of IGO to confirm such character. Regardless of the In concentration, there are three PL peaks around the 403 nm, 537 nm, and 710 nm, respectively. The peak centered at 403 nm due to the recombination of a trapped electron in a donor with a trapped hole in an acceptor, where the origins of the donor and acceptor are the V_O and the self-trapped hole and Ga-O vacancy pair, respectively. The peak centered at 537 nm is caused by the self-trapped hole and Ga-O vacancy pair, and the peak centered at the 719 nm is attributed to the V_Os, as exhibited in Figure S2. In addition, the peak intensity around 719 nm continuously increases with the increasing C_{In}, suggesting the enlarged V_O concentration induced by In dopant.

To further unveil the film characters, the Ga 3d and O 1s of different In concentrations are analyzed via XPS spectra. Figure 3(a)-(e) shows the O 1s spectra of films with different In concentrations (C_{In}). In particularly, the peaks of the O 1s are located at $\sim$ 530.8 eV and $\sim$ 531.9 eV. For all IGO films, the lower binding energy centered at $\sim$ 530.8 eV should be attributed to metal oxygen lattices (M-O). While the higher binding energy ($\sim$ 531.9 eV) is related to the residual metal hydroxide species coupling with oxygen vacancies (V_O+M-OH). Figure 3(f) exhibits that M-O have the relationship with V_O+M-OH. It can be inferred that all IGO films possess large amounts of oxygen vacancies (V_O) and metal hydroxide (M-OH). This is mainly due to the low annealing temperature caused incomplete conversion. Meanwhile, the V_O concentration increased when increasing the C_{In}, as can be seen from Figure 3(f), since In-O has a higher formation energy compared to Ga-O. This is consistent with the above DFT analysis and PL results. In fact, the carrier mobility of metal oxide films is related to oxygen vacancies and metal oxygen lattices. The metal oxygen lattices can contribute to trap sites reduction, which can induce high concentration of free electron. Meanwhile, at high carrier concentration, the free electrons generated
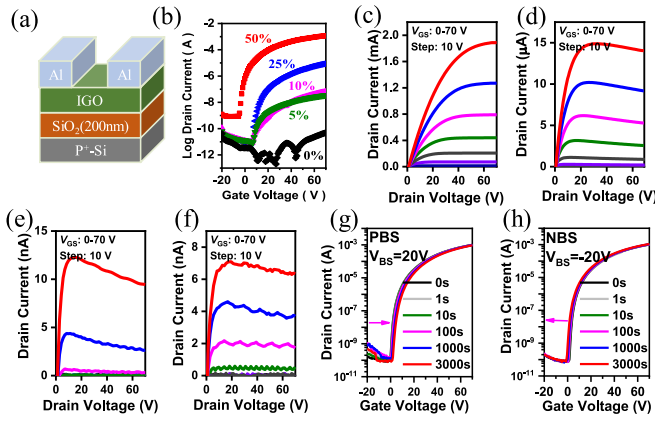
FIGURE 4. (a) Schematic of the thin film transistor structure. (b) Transfer characteristics of transistors based on different C_{In} films at V_{DS} = 30 V annealed at 450°C. Output characteristics of IGO TFTs with C_{In} of (c) 50 %, (d) 25 %, (e) 10 % and (f) 5 %. (g) Positive gate bias and (h) Negative gate bias test result for IGO (C_{In} = 50 %) TFT.

TABLE 1. Electrical parameters of IGO TFTs with different C_{In} (molar ratios) with a thermal annealing temperature of 450 °C.

C_{In}	μ_{sat} $(cm^2V^{-1}s^{-1})$	V_{TH} (V)	$I_{on/off}$	SS (V DECADE-1)	N_t $(cm^{-2}eV^{-1})$
0%	-	-	-	-	-
5%	1.7×10^{-4}	20	~10^4	3.24	3.40×10^{12}
10%	2.9×10^{-4}	20	~10^4	2.79	3.07×10^{12}
25%	4.2×10^{-2}	17.5	~10^6	1.52	2.13×10^{12}
50%	3.63	2.5	~10^6	1.38	2.02×10^{12}

by oxygen vacancies can enhance carrier transport by filling trap states, which is conducive to improving the mobilities of the IGO films. The ratios of In content in different IGO films are also confirmed by XPS measurements (Table S1), in the supplementary material. The results show that the ratio of In to Ga is almost similar to the precursor used.

In order to explore the feasibility of IGO films as channel layers, the structure of P^+-Si/SiO$_2$/IGO was successfully manufactured (Figure 4(a)). And all resulted films are annealed at 450 °C for 1h. The transfer characteristic curve of the IGO thin film transistors is presented in Figure 4(b). The output characteristics of the optimized IGO TFT based on different chemical components are shown in Figure 4(c)-(f). Table 1 presents the electronic parameters of different IGO TFTs, such as the field-effect mobility (μ_{sat}), the threshold voltage (V_{th}), the current on-off ratio ($I_{on/off}$), SS value, and interface trap density (N_t). All IGO TFTs exhibit typical n-channel transistor behaviors. The TFTs based on pristine Ga$_2$O$_3$ film (C_{In} = 0 %) are inactive, as is expected. However, the TFT devices exhibit improved performance when increasing the indium doping ratio. Especially the TFT based on IGO film with C_{In} = 50 % exhibits the best electronic performance with μ_{sat} of 3.63 cm^{2}V^{-1}s^{-1}, V_{th} of 2.5 V, $I_{on/off}$ of 10^6 and SS of 1.38 V decade^{-1} at V_{DS} = 30 V. The transfer characteristics of transistor based

on C_{In} = 50 % films in the dark and light are also described in Fig. S3 at V_{DS} = 30 V. The persistent light has almost no effect on the IGO (C_{In} = 50%) device, mainly because the sample contains a large content of Ga$_2$O$_3$ [26],[36]. After systematically analyzing the operating characteristics of the device, the bias stress stability of the best performance IGO (C_{In} = 50 %) TFT is also tested (Figure 4(g) and (h)). Under the action of 20 V positive gate bias for 3000 s, the ΔV_{TH} is 2.27 V. When -20 V negative gate bias is applied for 3000 s, the ΔV_{TH} is -1.95 V. The corresponding performance parameters are listed in Table S2 under different gate bias voltages. The IGO (C_{In} = 50 %) TFT demonstrates good bias stress stability characteristics with small ΔV_{TH} value. It is because Ga-O bonding is much stronger than In-O bonding, and it could suppress the oxygen vacancy formation caused by In doping. Hence, Ga has been used in the IZO or In$_2$O$_3$ system to enhance the film stability, which is similar with some other transition metals like Zr, Hf etc. [37]. The results show that In doping enables TFTs active based on solution processed low-temperature annealed amorphous gallium oxide thin film.

IV. CONCLUSION
In conclusion, we have developed a non-toxic, environment friendly, water-based technology to fabricate In-doped Ga$_2$O$_3$ TFTs. All the data indicate that In doping is beneficial to improve the electron mobility and decrease the annealing temperature of gallium oxide. Especially, the TFT based on IGO film with C_{In} = 50 % exhibits good electrical performance with μ_{sat} of 3.63 cm^{2}V^{-1}s^{-1}, V_{th} of 2.5 V, $I_{on/off}$ of 10^6 and SS of 1.38 V decade^{-1} at V_{DS} of 30 V. All the measurements provide a comprehensive study on the evolution of the energy band, optical properties and electrical performance of In-doped Ga$_2$O$_3$ thin film materials, which will promote further research on the application of Ga$_2$O$_3$ TFTs.

REFERENCES
[1] L. Liu, S. Chen, X. Liang, and Y. Pei, "Solution processed AlInO/In$_2$O$_3$ heterostructure channel thin film transistor with enhanced performance," *Adv. Electron. Mater.*, vol. 5, no. 12, Dec. 2019, Art. no. 1900550, doi: 10.1002/aelm.201900550.

[2] J. Chang, Z. Lin, M. Lin, C. Zhu, J. Zhang, and J. Wu, "Solution processed F doped ZnO (ZnO:F) for thin film transistors and improved stability through co-doping with alkali metals," *J. Mater. Chem. C*, vol. 3, no. 8, pp. 1787–1793, 2015, doi: 10.1039/C4TC02257B.

[3] Y. Jung, W. Yang, C. Y. Koo, K. Song, and J. Moon, "High performance and high stability low temperature aqueous solution-derived Li–Zr co-doped ZnO thin film transistors," *J. Mater. Chem.*, vol. 22, no. 12, p. 5390, 2012, doi: 10.1039/c2jm15526e.

[4] Y.-H. Lin *et al.*, "High electron mobility thin-film transistors based on solution-processed semiconducting metal oxide heterojunctions and quasi-superlattices," *Adv. Sci.*, vol. 2, no. 7, Jul. 2015, Art. no. 1500058, doi: 10.1002/advs.201500058.

[5] B. Wang *et al.*, "Solution-processed all-oxide transparent high-performance transistors fabricated by spray-combustion synthesis," *Adv. Electron. Mater.*, vol. 2, no. 4, Apr. 2016, Art. no. 1500427, doi: 10.1002/aelm.201500427.

[6] J. H. Park *et al.*, "Structural and electrical properties of solution-processed gallium-doped indium oxide thin-film transistors," *Jpn. J. Appl. Phys.*, vol. 50, no. 8, Aug. 2011, Art. no. 080202, doi: 10.1143/JJAP.50.080202.

[7] A. Liu *et al.*, "Solution combustion synthesis: Low-temperature processing for p-type Cu: NiO thin films for transparent electronics," *Adv. Mater.*, vol. 29, no. 34, 2017, Art. no. 1701599, doi: 10.1002/adma.201701599.

[8] K. H. Kim, Y.-H. Kim, H. J. Kim, J.-I. Han, and S. K. Park, "Fast and stable solution-processed transparent oxide thin-film transistor circuits," *IEEE Electron Device Lett.*, vol. 32, no. 4, pp. 524–526, Apr. 2011, doi: 10.1109/LED.2011.2107494.

[9] S. Jeong, Y.-G. Ha, J. Moon, A. Facchetti, and T. J. Marks, "Role of gallium doping in dramatically lowering amorphous-oxide processing temperatures for solution-derived indium zinc oxide thin-film transistors," *Adv. Mater.*, vol. 22, no. 12, pp. 1346–1350, Mar. 2010, doi: 10.1002/adma.200902450.

[10] J. Chang, Z. Lin, C. Zhu, C. Chi, J. Zhang, and J. Wu, "Solution-processed LiF-doped ZnO films for high performance low temperature field effect transistors and inverted solar cells," *ACS Appl. Mater. Interfaces*, vol. 5, no. 14, pp. 6687–6693, Jul. 2013, doi: 10.1021/am4014488.

[11] J. Chang, K. L. Chang, C. Chi, J. Zhang, and J. Wu, "Water induced zinc oxide thin film formation and its transistor performance," *J. Mater. Chem. C*, vol. 2, no. 27, pp. 5397–5403, 2014, doi: 10.1039/C3TC32311K.

[12] X. Yu, T. J. Marks, and A. Facchetti, "Metal oxides for optoelectronic applications," *Nat. Mater.*, vol. 15, no. 4, pp. 383–396, Apr. 2016, doi: 10.1038/nmat4599.

[13] X. Guo *et al.*, "Low temperature combustion synthesized indium oxide electron transport layer for high performance and stable perovskite solar cells," *J. Power Sources*, vol. 438, Oct. 2019, Art. no. 226981, doi: 10.1016/j.jpowsour.2019.226981.

[14] H.-C. Cheng, C.-F. Chen, and C.-Y. Tsay, "Transparent ZnO thin film transistor fabricated by sol-gel and chemical bath deposition combination method," *Appl. Phys. Lett.*, vol. 90, no. 1, Jan. 2007, Art. no. 012113, doi: 10.1063/1.2404590.

[15] G. X. Liu *et al.*, "High-performance fully amorphous bilayer metal-oxide thin film transistors using ultra-thin solution-processed ZrOx dielectric," *Appl. Phys. Lett.*, vol. 105, no. 11, Sep. 2014, Art. no. 113509. doi: 10.1063/1.4895782.

[16] W. Xu, H. Li, J.-B. Xu, and L. Wang, "Recent advances of solution-processed metal oxide thin-film transistors," *ACS Appl. Mater. Interfaces*, vol. 10, no. 31, pp. 25878–25901, Aug. 2018, doi: 10.1021/acsami.7b16010.

[17] W. Xu, H. Cao, L. Liang, and J. B. Xu, "Aqueous solution-deposited gallium oxide dielectric for low-temperature, low-operating-voltage indium oxide thin-film transistors: A facile route to green oxide electronics," *ACS Appl. Mater. Interfaces*, vol. 7, no. 27, pp. 14720–14725, 2015, doi: 10.1021/acsami.5b02451.

[18] D.-H. Lee, Y.-J. Chang, G. S. Herman, and C.-H. Chang, "A general route to printable high-mobility transparent amorphous oxide semiconductors," *Adv. Mater.*, vol. 19, no. 6, pp. 843–847, Mar. 2007, doi: 10.1002/adma.200600961.

[19] S. R. Thomas *et al.*, "High electron mobility thin-film transistors based on Ga₂O₃ grown by atmospheric ultrasonic spray pyrolysis at low temperatures," *Appl. Phys. Lett.*, vol. 105, no. 9, Sep. 2014, Art. no. 092105, doi: 10.1063/1.4894643.

[20] J. L. Hudgins, G. S. Simin, E. Santi, and M. A. Khan, "An assessment of wide bandgap semiconductors for power devices," *IEEE Trans. Power Electron.*, vol. 18, no. 3, pp. 907–914, May 2003, doi: 10.1109/TPEL.2003.810840.

[21] J. Bae, H. W. Kim, I. H. Kang, G. Yang, and J. Kim, "High breakdown voltage quasi-two-dimensional β-Ga₂O₃ field-effect transistors with a boron nitride field plate," *Appl. Phys. Lett.*, vol. 112, no. 12, Mar. 2018, Art. no. 122102, doi: 10.1063/1.5018238.

[22] J. Su *et al.*, "Unusual electronic and optical properties of two-dimensional Ga₂O₃ predicted by density functional theory," *J. Phys. Chem. C*, vol. 122, no. 43, pp. 24592–24599, Nov. 2018, doi: 10.1021/acs.jpcc.8b08650.

[23] R. Guo *et al.*, "Understanding the potential of 2D Ga₂O₃ in flexible optoelectronic devices: Impact of uniaxial strain and electric field," *Adv. Theory Simulat.*, vol. 2, no. 9, Sep. 2019, Art. no. 1900106, doi: 10.1002/adts.201900106.

[24] R. Guo *et al.*, "Surface functionalization modulates the structural and optoelectronic properties of two-dimensional Ga₂O₃," *Mater. Today Phys.*, vol. 12, Mar. 2020, Art. no. 100192, doi: 10.1016/j.mtphys.2020.100192.

[25] G. Gonçalves *et al.*, "High mobility a-IGO films produced at room temperature and their application in TFTs," *Electrochem. Solid-State Lett.*, vol. 13, no. 1, p. H20, 2010, doi: 10.1149/1.3257613.

[26] A. Olziersky *et al.*, "Role of Ga₂O₃–In₂O₃–ZnO channel composition on the electrical performance of thin-film transistors," *Mater. Chem. Phys.*, vol. 131, nos. 1–2, pp. 512–518, Dec. 2011, doi: 10.1016/j.matchemphys.2011.10.013.

[27] S. R. Thomas *et al.*, "High electron mobility thin-film transistors based on Ga₂O₃grown by atmospheric ultrasonic spray pyrolysis at low temperatures," *Appl. Phys. Lett.*, vol. 105, no. 9, Sep. 2014, Art. no. 092105, doi: 10.1063/1.4894643.

[28] Y. G. Kim, T. Kim, C. Avis, S. H. Lee, and J. Jang, "Stable and high-performance indium oxide thin-film transistor by Ga doping," *IEEE Trans. Electron Devices*, vol. 63, no. 3, pp. 1078–1084, Mar. 2016, doi: 10.1109/TED.2016.2518703.

[29] Z. Lin, J. Chang, C. Zhang, J. Zhang, J. Wu, and Y. Hao, "Low temperature aqueous solution-processed Li doped ZnO buffer layers for high performance inverted organic solar cells," *J. Mater. Chem. C*, vol. 4, no. 25, pp. 6169–6175, 2016, doi: 10.1039/C6TC00760K.

[30] A. A. Adllan and A. D. Corso, "Ultrasoft pseudopotentials and projector augmented-wave data sets: Application to diatomic molecules," *J. Phys. Condens. Matter.*, vol. 23, no. 42, Oct. 2011, Art. no. 425501, doi: 10.1088/0953–8984/23/42/425501.

[31] R. A. Vargas−Hernández, "Bayesian optimization for calibrating and selecting hybrid-density functional models," *J. Phys. Chem. A*, vol. 124, no. 20, pp. 4053–4061, May 2020, doi: 10.1021/acs.jpca.0c01375.

[32] J. P. Perdew, K. Burke, and M. Ernzerhof, "Generalized gradient approximation made simple," *Phys. Rev. Lett.*, vol. 77, no. 18, pp. 3865–3868, Oct. 1996, doi: 10.1103/PhysRevLett.77.3865.

[33] L. Feng, J. Su, S. Chen, and Z. Liu, "First-principles investigations on vacancy formation and electronic structures of monolayer MoS2," *Mater. Chem. Phys.*, vol. 148, nos. 1–2, pp. 5–9, Nov. 2014, doi: 10.1016/j.matchemphys.2014.07.026.

[34] C. Fares *et al.*, "Valence band offsets for CuI on (-201) bulk Ga₂O₃ and epitaxial (010) (Al₀.₁₄Ga₀.₈₆)₂O₃," *Appl. Phys. Lett.*, vol. 113, no. 18, Oct. 2018, Art. no. 182101, doi: 10.1063/1.5055941.

[35] L. Chang, Y. Sung, J. Yeh, and H. C. Shih, "Enhanced optoelectronic performance from the Ti-doped ZnO nanowires," *J. Appl. Phys.*, vol. 109, no. 7, Apr. 2011, Art. no. 074318, doi: 10.1063/1.3554686.

[36] S. Jeon *et al.*, "Gated three-terminal device architecture to eliminate persistent photoconductivity in oxide semiconductor photosensor arrays," *Nat. Mater.*, vol. 11, no. 4, pp. 301–305, Apr. 2012, doi: 10.1038/nmat3256.

[37] F. Jaehnike, D. V. Pham, C. Bock, and U. Kunze, "Role of gallium and yttrium dopants on the stability and performance of solution processed indium oxide thin-film transistors," *J. Mater. Chem. C*, vol. 7, no. 25, pp. 7627–7635, 2019, doi: 10.1039/C8TC06270F.